Sangamesh R. Deepak
Department of Mechanical Engineering,
Indian Institute of Science,
Bangalore 560012, India
e-mail: sangu@mecheng.iisc.ernet.in

Amrith N. Hansoge
Department of Mechanical Engineering,
Indian Institute of Science,
Bangalore 560012, India
e-mail: amrithnh@mecheng.iisc.ernet.in

G. K. Ananthasuresh
Department of Mechanical Engineering,
Indian Institute of Science,
Bangalore 560012, India
e-mail: suresh@mecheng.iisc.ernet.in

Application of Rigid-Body-Linkage Static Balancing Techniques to Reduce Actuation Effort in Compliant Mechanisms

There are analytical methods in the literature where a zero-free-length spring-loaded linkage is perfectly statically balanced by addition of more zero-free-length springs. This paper provides a general framework to extend these methods to flexure-based compliant mechanisms through (i) the well know small-length flexure model and (ii) approximation between torsional springs and zero-free-length springs. We use first-order truncated Taylor's series for the approximation between the torsional springs and zero-free-length springs so that the entire framework remains analytical, albeit approximate. Three examples are presented and the effectiveness of the framework is studied by means of finite-element analysis and a prototype. As much as 70% reduction in actuation effort is demonstrated. We also present another application of static balancing of a rigid-body linkage by treating a compliant mechanism as the spring load to a rigid-body linkage.
[DOI: 10.1115/1.4031192]

1 Introduction

Compliant mechanisms [1] are single monolithic elastic bodies that transform and/or transmit motion and forces. Unlike rigid-body linkages, where the deformation is due to joints, compliant mechanisms rely upon elastic deformation. Because of the elastic deformation, effort is required to actuate compliant mechanisms even when they are not acting on any workpiece or against any load. Reduction or elimination of the actuation effort saves actuation energy and also improves force feedback characteristics of compliant graspers [2]. Since elimination of the effort over a range of configurations is equivalent to having static equilibrium over that range, these phenomena are referred to as *static balance* [2].

Various strategies have been investigated for the design of statically balanced compliant mechanisms. While some of them are specifically directed toward designing laparoscopic graspers [2–5], many address the static balancing strategies for general compliant mechanisms [6–12]. An overview of different criteria that could be used to design a statically balanced compliant mechanism is described in Ref. [9].

In Refs. [4,7,10,12], static balancing relies on the design of a distinct negative stiffness balancer. We know that negative stiffness is associated with unstable equilibrium. While the authors of Ref. [12] used their previous work on multistable compliant mechanisms, prestressed slider crank linkage and a column under compression formed the basis for obtaining unstable equilibrium in Refs. [4,7,10]. Optimization, including topology optimization [4], was used to increase the accuracy of static balancing.

Herder [13,14] introduced a new class of problems wherein a rigid-body linkage under a spring load is to be statically balanced by adding one or more balancing springs. References [13] and [15] dealt with perfect static balancing of a four-bar linkage where both original and balancing springs are of zero-free-length. When both original and balancing springs are of zero-free-length, it was shown in Refs. [16,17] that any revolute-jointed rigid-body linkage can be perfectly balanced. Furthermore, it was suggested in Ref. [15] that since flexure-based compliant mechanisms can be approximated as *torsional*-spring-loaded rigid-body linkages, study of static balancing of spring-loaded rigid-body linkages holds relevance for compliant mechanisms as well.

With an intent to apply on compliant mechanisms through small-length flexure model, Radaelli et al. [18] focused on developing approximate static balancing strategies for rigid-body linkages where both original and balancing springs are of torsional type. While authors of Refs. [13–15,17] gave perfect static balancing methods based on simple analytical equations, Radaelli et al. [18] relied on genetic algorithm-based numerical optimization and visual judgment of three-dimensional graphs. The work of Radaelli et al. [18] was followed up by its application on static balancing of a two degree-of-freedom compliant mechanism, which has a self-guided straight line motion [6].

In order to conceptualize an approximately statically balanced compliant mechanism without resorting to numerical procedures, we link the methods in Refs. [13–17] to small-length flexure-based compliant mechanisms by an intermediate step. The intermediate step is the approximation of torsional springs, which models small-length flexures, by zero-free-length springs. The approximation is based on matching terms up to first-order terms in the Taylor's series expansion of actuator force or torque. This idea is formalized as a framework in Sec. 2.

There are parallel works on relating the insights gained from Ref. [14] to pseudo-rigid-body models of compliant mechanisms. Based on an example given in Ref. [14], a generic zero-stiffness spring was designed in Ref. [8]. The intent was to use such springs as building blocks for designing statically balanced compliant mechanisms. In the work, cross-axis flexural pivot was used as the compliant revolute joint, and cantilever type beam was used to emulate zero-free-length springs. The idea of generic zero-stiffness compliant joint was taken forward in Ref. [19], where a simple easy-to-use nondimensional equation was obtained for the design of zero-stiffness cross-axis flexural pivot. Compliant joints in a statically balanced system are usually subjected to very high compressive loads. Through the example of cross-axis flexural pivot, it was brought to the fore in Ref. [19] that the stiffness of

Manuscript received January 4, 2015; final manuscript received July 21, 2015; published online November 24, 2015. Assoc. Editor: Larry L. Howell.

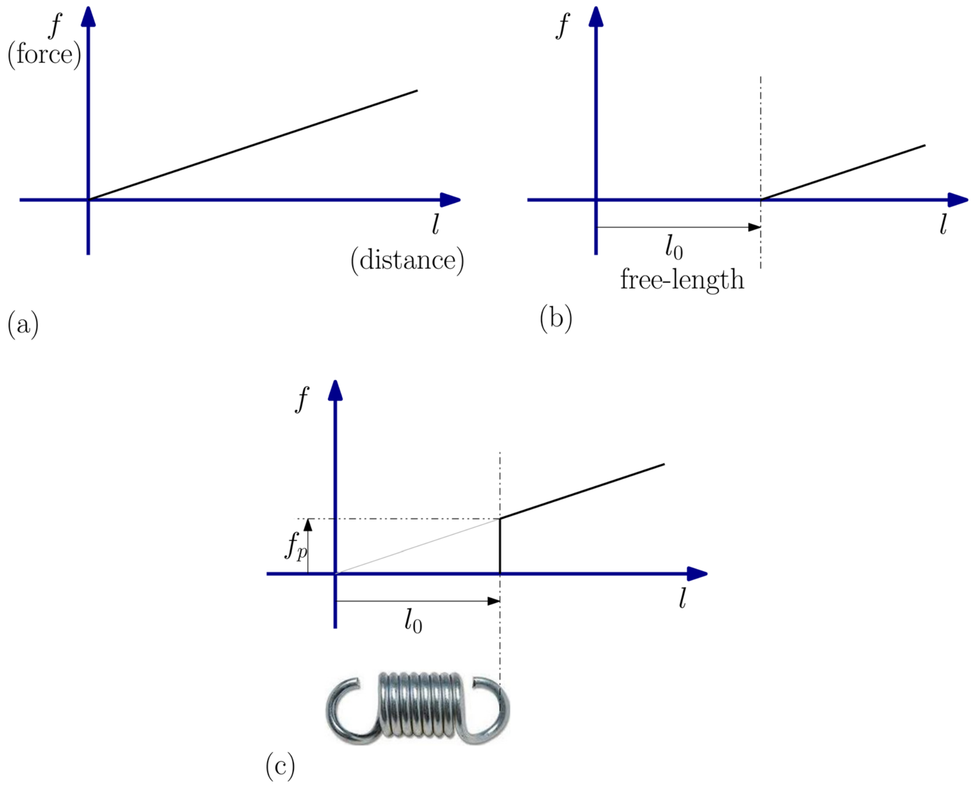

Fig. 1 Practically realizing a zero-free-length spring by giving appropriate pretension: (*a*) zero free length, (*b*) shifting of the plot along *l*-axis by l_0, and (*c*) shifting of the plot along *f*-axis due to prestressing f_p

the compliant joint changes due to high compressive loads. To account for the change, corrections have to be applied to the balancing spring parameters.

Apart from presenting the analytical framework in Sec. 2, we also demonstrate an example in Sec. 3, where a reduction in actuation effort is accomplished by adding a spring-loaded rigid-body linkage rather than just springs. Since the analytical spring-load balancing techniques for rigid-body linkages and the torsional-spring-loaded rigid-body linkage approximations of compliant mechanisms are crucial to our approach, we briefly describe them next.

1.1 Exact Static Balancing for Spring-Loaded Rigid-Body Linkages. A method to statically balance any pin-jointed linkage loaded by zero-free-length springs is given in Ref. [17]. Ideally, in a zero-free-length spring, the two anchor points are coincident when the force on the spring is zero. A plot of the force on the spring (f) versus the distance between the anchor points (l) would be as shown in Fig. 1(*a*), where the plot is collinear with the origin. In reality, in a helical spring, the two anchor points can never be coincident because of the finite volume of the spring. In the absence of force on the spring, the distance between the anchor points, i.e., free-length, is finite. The effect of the free-length is to shift f versus l plot along the l-axis, as shown in Fig. 1(*b*). There is another factor that affects the plot—prestress, which can be introduced by cold working. Prestress shifts the plot along the f-axis, as shown in Fig. 1(*c*). By introducing appropriate prestress, the f versus l plot can be made collinear with the origin and in the working range, i.e., l greater than free-length, the plot is the same as that in Fig. 1(*a*).

In this paper, we apply the method of Deepak and Ananthasuresh [17] to a pin-jointed lever and a double pin-jointed linkage. Hence, it is apt to summarize the result of the paper [17] as applied to these two linkages.

1.1.1 Double Pin-Jointed Linkages. In the double pin-jointed linkage shown in Fig. 2, there are two bodies labeled as 1 and 2 in addition to the ground that is labeled as 0. Attached to bodies 1 and 2 are zero-free-length springs anchored from the ground. There are local coordinate frames associated with bodies 1 and 2, as shown in Fig. 2. Let $\mathcal{Z}_i^{[j]}$ represent the ith spring attached to the

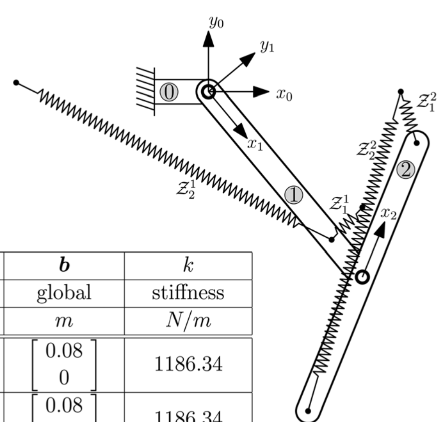

spring	$\boldsymbol{a}$	$\boldsymbol{b}$	k
	local	global	stiffness
	m	m	N/m
$\mathcal{Z}_1^2$	$\begin{bmatrix} 0.06 \\ 0 \end{bmatrix}$	$\begin{bmatrix} 0.08 \\ 0 \end{bmatrix}$	1186.34
$\mathcal{Z}_2^2$	$\begin{bmatrix} -0.06 \\ 0 \end{bmatrix}$	$\begin{bmatrix} 0.08 \\ 0 \end{bmatrix}$	1186.34
coordinates of pivot of (1 to 2) revolute joint $\boldsymbol{s} = \begin{bmatrix} 0.1 \\ 0 \end{bmatrix}$			
$\mathcal{Z}_1^1$	$\begin{bmatrix} 0.08 \\ 0 \end{bmatrix}$	$\begin{bmatrix} 0.064 \\ -0.048 \end{bmatrix}$	148.28
$\mathcal{Z}_2^1$	$\begin{bmatrix} 0.08 \\ 0 \end{bmatrix}$	$\begin{bmatrix} -0.08 \\ 0.0035 \end{bmatrix}$	3151.22

Fig. 2 A double pin-jointed linkage under the zero-free-length spring loads

jth body. Associated with each spring $\mathcal{Z}_i^{[j]}$ are the parameters $\boldsymbol{a}_i^{[j]}$, $\boldsymbol{b}_i^{[j]}$, and $k_i^{[j]}$, which represent the local coordinates of the attachment point on body j, global coordinates (with respect to the ground frame) of the anchor point on the ground (labeled as 0th body), and the spring constant. We represent the coordinates as 2×1 column matrix. Further, let n_j represent the total number of springs attached to body j. As per the results of Deepak and Ananthasuresh [17], obtained by setting the coefficients of the configuration-dependent functions in the expression for the potential energy to zero, the double pin-jointed linkage under the action of zero-free-length spring, $\mathcal{Z}_i^{[2]}$, $i = 1 \cdots n_2$, and $\mathcal{Z}_i^{[1]}$, $i = 1 \cdots n_1$ will be in perfect static balance over all the configurations of the linkage if

$$\sum_{i=1}^{n_2} k_i^{[2]} \boldsymbol{b}_i^{[2]^{\mathrm{T}}} \begin{bmatrix} 1 & 0 \\ 0 & 1 \end{bmatrix} \boldsymbol{a}_i^{[2]} = 0 \tag{1}$$

$$\sum_{i=1}^{n_2} k_i^{[2]} \boldsymbol{b}_i^{[2]^{\mathrm{T}}} \begin{bmatrix} 0 & -1 \\ 1 & 0 \end{bmatrix} \boldsymbol{a}_i^{[2]} = 0 \tag{2}$$

$$\sum_{i=1}^{n_2} k_i^{[2]} \boldsymbol{a}_i^{[2]} = 0 \tag{3}$$

$$\sum_{i=1}^{n_1} k_i^{[1]} \boldsymbol{b}_i^{[1]^{\mathrm{T}}} \begin{bmatrix} 1 & 0 \\ 0 & 1 \end{bmatrix} \boldsymbol{a}_i^{[1]} + \tilde{\boldsymbol{b}}^{\mathrm{T}} \begin{bmatrix} 1 & 0 \\ 0 & 1 \end{bmatrix} \boldsymbol{s} = 0 \tag{4}$$

$$\sum_{i=1}^{n_1} k_i^{[1]} \boldsymbol{b}_i^{[1]^{\mathrm{T}}} \begin{bmatrix} 0 & -1 \\ 1 & 0 \end{bmatrix} \boldsymbol{a}_i^{[1]} + \tilde{\boldsymbol{b}}^{\mathrm{T}} \begin{bmatrix} 0 & -1 \\ 1 & 0 \end{bmatrix} \boldsymbol{s} = 0 \tag{5}$$

where $\boldsymbol{s}$ represents the local coordinates (with respect to coordinate frame of body 1) of the point where body 1 joins with body 2 through a pin-joint, and $\tilde{\boldsymbol{b}}$ is given by

$$\tilde{\boldsymbol{b}} = \sum_{i=1}^{n_2} k_i^{[2]} \boldsymbol{b}_i^{[2]} \tag{6}$$

Apart from Eq. (3), which is a two-dimensional vector equation, rest of the equations are scalar equations. Equation (1) involves weighted sum of dot product of vectors. Equation (2) is the same as Eq. (1) except that one of the vectors is turned by right angle before taking the dot product. Equations (4) and (5) have similar nature. In total, there are six equations that spring parameters have to satisfy to ensure static balance.

As an example, consider the linkage in Fig. 2, where $\mathcal{Z}_1^{[2]}$ and $\mathcal{Z}_1^{[1]}$ be the original spring loads on the linkage, and we would want to balance the linkage by adding two springs $\mathcal{Z}_2^{[2]}$ and $\mathcal{Z}_2^{[1]}$. We would want to find the parameters of balancing springs—$\boldsymbol{a}_2^{[2]}$, $\boldsymbol{b}_2^{[2]}$, $k_2^{[2]}$, $\boldsymbol{a}_2^{[1]}$, $\boldsymbol{b}_2^{[1]}$, $k_2^{[1]}$ —as solutions to Eqs. (1)–(5). This constitutes a system of six scalar equations in ten unknowns, and it turns out to be underdetermined system of equations with non-unique solution.

We will first find the parameters of $\mathcal{Z}_2^{[2]}$ and then that of $\mathcal{Z}_2^{[1]}$. Equation (3) force $\boldsymbol{a}_2^{[2]}$ to be in opposite direction of $\boldsymbol{a}_1^{[2]}$ and inversely proportional in magnitude to their respective spring constants. By making a choice of $k_2^{[2]}$, $\boldsymbol{a}_2^{[2]}$ can be determined. With this, Eqs. (1) and (2) become linear equations in $\boldsymbol{b}_2^{[2]}$ and it can be solved. Now, $\tilde{\boldsymbol{b}}$ is found from Eq. (6). Further, by making a choice in the direction and magnitude of $\boldsymbol{a}_2^{[1]}$ and $k_2^{[1]}$, $\boldsymbol{b}_2^{[1]}$ can be solved from Eqs. (4) and (5). A feasible solution is presented in the table of Fig. 2.

The balancing procedure for a general linkage is similar to that of 2R linkage with the number of static balancing equations being roughly proportional to the number of links. Even though Ref. [17] suggests strategies to solve the equations, multiple solutions are inherent in the method. Hence, discretion of a designer for resolving multiple solutions is essential.

1.1.2 Pin-Jointed Lever. In the pin-jointed lever shown in Fig. 3, there is only one body, labeled as 1, which is attached to the ground (body 0) with a pin-joint. The zero-free-length springs attached from the ground to this body would be in static balance if they satisfy

$$\sum_{i=1}^{n_1} k_i^{[1]} \boldsymbol{b}_i^{[2]^{\mathrm{T}}} \begin{bmatrix} 1 & 0 \\ 0 & 1 \end{bmatrix} \boldsymbol{a}_i^{[1]} = 0 \tag{7}$$

$$\sum_{i=1}^{n_1} k_i^{[1]} \boldsymbol{b}_i^{[2]^{\mathrm{T}}} \begin{bmatrix} 0 & -1 \\ 1 & 0 \end{bmatrix} \boldsymbol{a}_i^{[1]} = 0 \tag{8}$$

These conditions were also obtained in Ref. [17] by setting the coefficient of the joint angle-dependent functions to zero. Again, as an illustration, the numerical parameters of the springs attached in Fig. 3 are given in the table of the same figure. It may be verified that the springs do satisfy Eqs. (7) and (8).

1.2 Small-Length Flexure-Based Compliant Mechanisms Approximated by Spring-Loaded Rigid-Body Linkages. Small-length flexure model is applicable to compliant mechanisms that are made up of flexures. One such compliant mechanism is shown in Fig. 4(*a*). The deformation in the mechanism occurs predominantly at the flexures with the remaining portion being rigid. Small-length flexure approximation [1,20] replaces the flexures by pin-joints with torsional springs, as shown in Fig. 4(*b*). In the undeformed configuration, center of the pin-joint coincides with the center of the flexure. Further, the torsional-spring constant is the same as ratio of moment to relative rotation between two ends of the flexure during a pure bending. This constant is evaluated using Euler–Bernoulli beam theory as EI/l, where E is the Young' modulus, I is the moment of inertia of the cross section of the flexure, and l is the length of the flexure. The derivation of the constant is also shown in Fig. 4(*c*).

2 An Analytical Framework

We propose an analytical framework for using rigid-body-linkage static balancing techniques on flexure-based compliant mechanisms. We first apply the framework on a flexure beam shown in Fig. 5 and follow it with a summary of the framework.

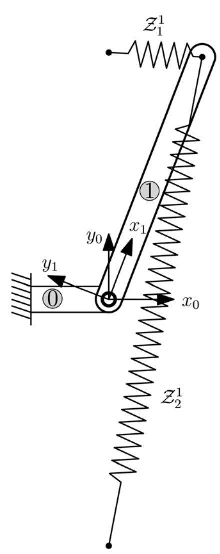

spring	$\boldsymbol{a}$	$\boldsymbol{b}$	k
	local	global	stiffness
	m	m	N/m
$\mathcal{Z}_1^1$	$\begin{bmatrix} 0.2 \\ 0 \end{bmatrix}$	$\begin{bmatrix} 0 \\ 0.2 \end{bmatrix}$	35.6
$\mathcal{Z}_2^1$	$\begin{bmatrix} 0.2 \\ 0 \end{bmatrix}$	$\begin{bmatrix} 0 \\ -0.2 \end{bmatrix}$	35.6

Fig. 3 A pin-jointed lever under the zero-free-length spring loads

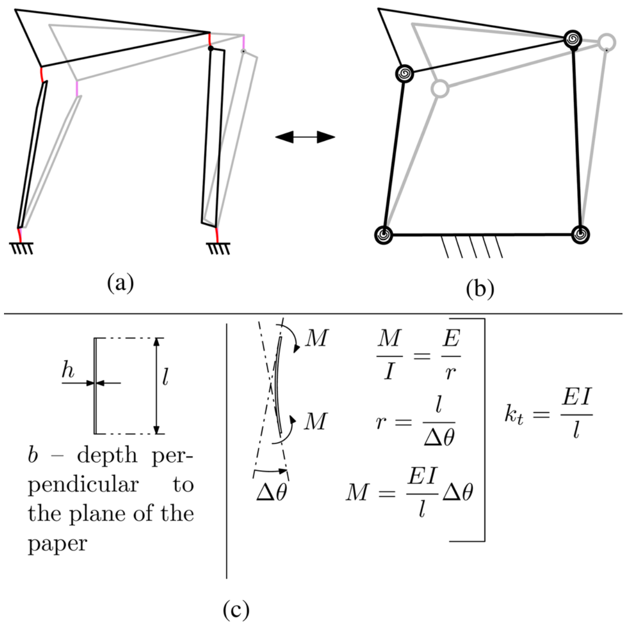

Fig. 4 Rigid-body linkage approximation of a flexure-based compliant mechanism

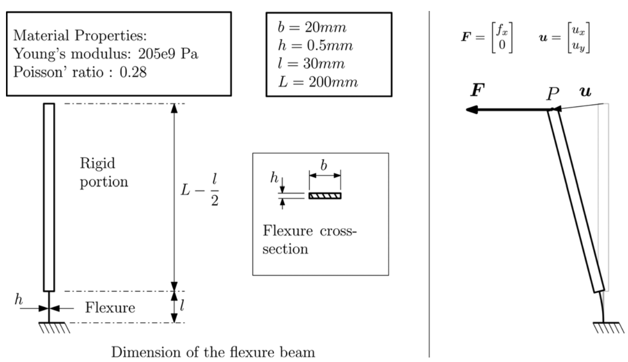

Fig. 5 A flexure-based lever

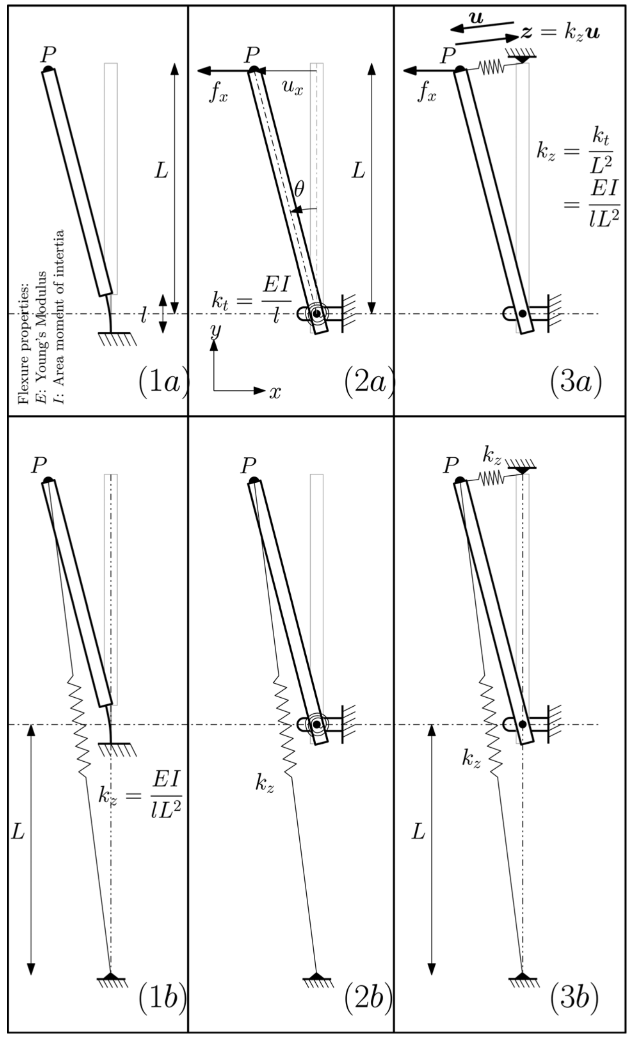

Fig. 6 Various cases in the analytical framework that is applied to the flexure beam

2.1 Static Balancing of a Flexure Beam. The analytical framework should reduce the effort involved in the actuation of a compliant mechanism. Various functions can be taken to characterize this effort. In the flexure beam of Fig. 5, f_x versus u_x may be taken to characterize the effort, where u_x is the horizontal displacement of the top tip P when a horizontal force f_x is applied at the tip. After applying the analytical framework, we expect f_x to get reduced to a very small percent of its original value over a range of values of u_x.

In order to apply rigid-body static balancing techniques, we apply small-length flexure approximation to obtain a torsional-spring-loaded lever as shown in Fig. 6(2*a*). Since the static balancing technique of Deepak and Ananthasuresh [17] is to be applied on a linkage loaded with zero-free-length springs, we next approximate the torsional spring by a zero-free-length spring as shown in Fig. 6(3*a*). For convenience, we refer to situations in various subfigures of Fig. 6 as case (#x), where (#x) is the subfigure label. The parameters of the zero-free-length spring in case (3a) are found based on matching f_x versus u_x function between cases (2a) and (3a). In this paper, we base this match on having the constant term and the first-order term of the Taylor's expansion being the same. In other words, f_x and df_x/du_x at $u_x = 0$ being the same in the two cases is the criteria for finding the parameters of the zero-free-length spring. The significance of this choice will be discussed later.

Consider case (2a). When external force f_x acts on the linkage at P, this will be in equilibrium with the torque exerted by the torsional spring. From virtual work principle we have

$$0 = -k_t\theta\delta\theta + f_x\delta u_x \tag{9}$$

where δu_x is the virtual displacement corresponding to virtual tilt $\delta\theta$ (see Fig. 6(2*a*)). From Eq. (9), we have

$$f_x = k_t\theta\frac{d\theta}{du_x} \tag{10}$$

By differentiating f_x with respect to θ, we get

$$\frac{df_x}{d\theta} = k_t\frac{d\theta}{du_x} + k_t\theta\frac{d}{d\theta}\left(\frac{d\theta}{du_x}\right) \tag{11}$$

In the initial configuration, i.e., at $\theta = 0$, from Eqs. (10) and (11), we have

$$f_x = 0, \quad \frac{df_x}{d\theta} = k_t\frac{d\theta}{du_x} \quad \text{and} \quad \frac{df_x}{du_x} = \frac{df_x}{d\theta}\frac{d\theta}{du_x} = k_t\left(\frac{d\theta}{du_x}\right)^2 \tag{12}$$

All the quantities can be easily found through velocity analysis of linkages [21]. In particular, $d\theta/du_x$ is $1/L$. Hence, for case (2a), at the reference configuration ($\theta = 0$) we have

$$f_x = 0 \qquad \text{and} \qquad \frac{df_x}{du_x} = \frac{k_t}{L^2} \tag{13}$$

Consider case (3a). We incorporate one zero-free-length spring such that in the reference configuration, the spring is undeformed just as the torsional spring in case (2a) is undeformed in the reference configuration. If the anchor point of the zero-free-length spring is chosen to be at P, as shown in Fig. 6(3*a*), then the anchor point on the ground is the position of point P in the reference configuration. We have to find its spring constant, which is labeled as k_z. Similar to case (2a), for equilibrium, we have

$$0 = -k_z \boldsymbol{u} \cdot \delta \boldsymbol{u} + f_x \delta u_x \tag{14}$$

Hence,

$$f_x = k_z \boldsymbol{u} \cdot \frac{d\boldsymbol{u}}{du_x} = k_z \left(u_x + u_y \frac{du_y}{du_x} \right) \tag{15}$$

and

$$\frac{df_x}{du_x} = k_z \left(1 + u_y \frac{d}{du_x} \left(\frac{du_y}{du_x} \right) + \left(\frac{du_y}{du_x} \right)^2 \right) \tag{16}$$

At the reference configuration, $u_x = 0$, $u_y = 0$ and from velocity analysis of linkages, $du_y/du_x = 0$. Therefore, at the reference configuration, we have

$$f_x = 0 \qquad \text{and} \qquad \frac{df_x}{du_x} = k_z \tag{17}$$

By imposing that f_x and df_x/du_x match between cases (2a) and (3a), we solve for k_z as k_t/L^2. The zero-free-length spring-loaded lever can be statically balanced by adding another zero-free-length spring, as shown in Fig. 6(3*b*). The theory behind this was explained in Sec. 1.1.2 along with an illustration in Fig. 3. Note that the illustration was selected so as to be applicable to case (3b).

Just as the addition of a balancing spring to case (3a) resulted in a perfectly statically balanced case (3b), we expect that the addition of the same balancing spring to case (1a) should result in case (1b) that is approximately statically balanced. The reason for such an expectation is that case (3a) approximates the flexure beam of case (1a) in terms of both kinematics and elastostatics. The function f_x versus u_x, which we have chosen as a metric to judge the static balance, is plotted in Fig. 7 for both cases (1a) and (1b) over a range of values of u_x. The plot was obtained by large-displacement linear elastic finite-element analysis using COMSOL software. The numerical values for the parameters of the flexure beam are as in Fig. 5. From the plot, it may be seen that the f_x has decreased to less than 30% of its original value. The length of the range of u_x is 0.1 m in comparison to $2L = 0.4$ m, the largest dimension of the overall arrangement in case (1b).

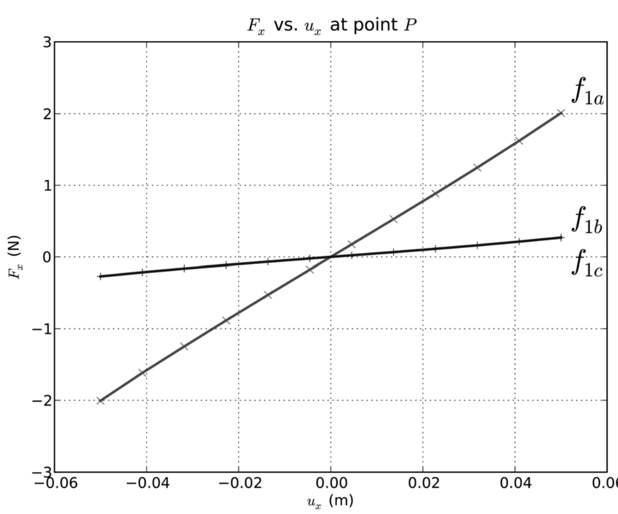

Fig. 7 $\boldsymbol{f_x}$ **versus** $\boldsymbol{u_x}$ **before (1a) and after (1b) application of the analytical framework**

One may improve the percentage of decrease by further optimizing the balancing parameters. However, as discussed later, the intent of this analytical framework is to provide simple tools for *conceptualization* of statically balanced configuration which may be later optimized for further improvements. Improvements could include replacing the zero-free-length springs by more practical normal springs or other compliant elements.

2.2 The Framework. Before we describe other examples, we briefly enunciate the steps involved in the analytical framework that can be applied for approximate static balance of a general flexure-based compliant mechanisms.

Step 1: Identification of an effort function. The function that we choose as a metric to judge the static balance, such as f_x versus u_x in Sec. 2.1, is labeled as effort function. Identifying a suitable effort function is the first step.
Step 2: Application of flexure approximation to the given flexure-based compliant mechanism (case (1a)) in order to obtain torsional-spring-loaded rigid-body linkage (case (2a)).
Step 3: Approximation of torsional springs by zero-free-length springs to obtain case (3b). This approximation is performed by having a match between cases (2a) and (3a) for the first few terms of Taylor expansion of the effort function.
Step 4: Application of static balancing methods that add only springs but not auxiliary links. This step results in perfectly balanced case (3b).
Step 5: Incorporation of balancing spring of case (3b) into case (1a) to obtain case (1b).

At the end of this framework, we will have zero-free-length springs attached to the flexure-based compliant mechanism. We now give two more illustrations that show the effectiveness of the framework toward approximate static balance.

2.3 A Compliant Four-Bar Linkage. Figure 8(1*a*) shows a compliant four-bar linkage both in the undeformed and a deformed configuration. There are four flexures and all of them have identical dimensions and elastic properties.

2.3.1 Step 1—Identification of Effort Function. E is a point at the end of one of the flexures, as shown in Fig. 8(1*a*). f_x versus u_x is taken as the effort function, where u_x is the horizontal displacement of point E for an applied horizontal force of magnitude f_x.

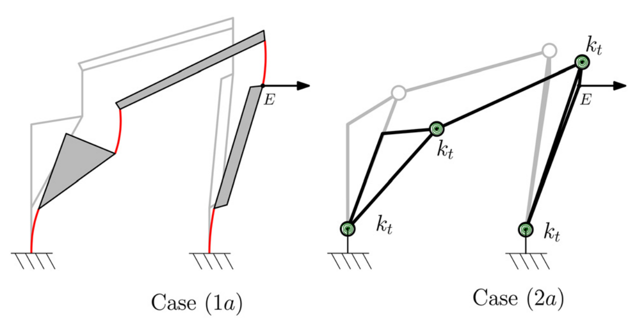

E	Young's modulus	$205e9[Pa]$
h	Height of the flexure cross-sections	$500e-6[m]$
b	Width of the flexure cross-sections	$4e-2[m]$
I	Area moment of inetria $= \frac{bh^3}{12}$	$4.167e-13[m^4]$
l	Length of the flexures	$3e-2[m]$
k_t	Torsional spring constant	$2.847[N-m/rad]$

Fig. 8 A compliant four-bar linkage—cases (1a) and (2a)

2.3.2 Step 2—Approximation With a Rigid-Body Linkage Loaded by Torsional Springs. Application of small-length flexure rigid-body linkage approximation to the compliant mechanism of case (1a) (Fig. 8(1*a*)) leads to case (2a), as shown in Fig. 8(2*a*). The details of the flexures of case (1a) and evaluation of torsional-spring constant of the torsional springs of case (2a) are given in the table of Fig. 8. In the undeformed configuration, the center of flexures in case (1a) and, hence, center of pivot joints in case (2a) form a quadrilateral, as shown in Fig. 9.

2.3.3 Step 3—Approximation of Torsional Springs by Zero-Free-Length Springs. It is proposed to approximate the four torsional springs of case (2a) by a single zero-free-length spring as in Fig. 10(3*a*). In the undeformed configuration, the zero-free-length spring has its two anchor points coincident at a height of 70 mm above the pivot center A. In order to find the spring constant of the spring, we find first two terms of the Taylor series expansion of f_x versus u_x relation in both cases (2a) and (3a).

When the rigid-body linkage of cases (2a) and (3a) moves away from the reference configuration, α_i, $i = 1 \cdots 4$ of the quadrilateral in Fig. 9 also change. Let these changes be represented as θ_i, $i = 1 \cdots 4$, respectively. θ_i, $i = 1 \cdots 4$ are also the angular deflections of the torsional springs at the pivots A, B, C, and D, respectively. For the linkage, under the action of the torsional springs and the applied horizontal force f_x at point E, the equilibrium equation, through virtual work principle, takes the form

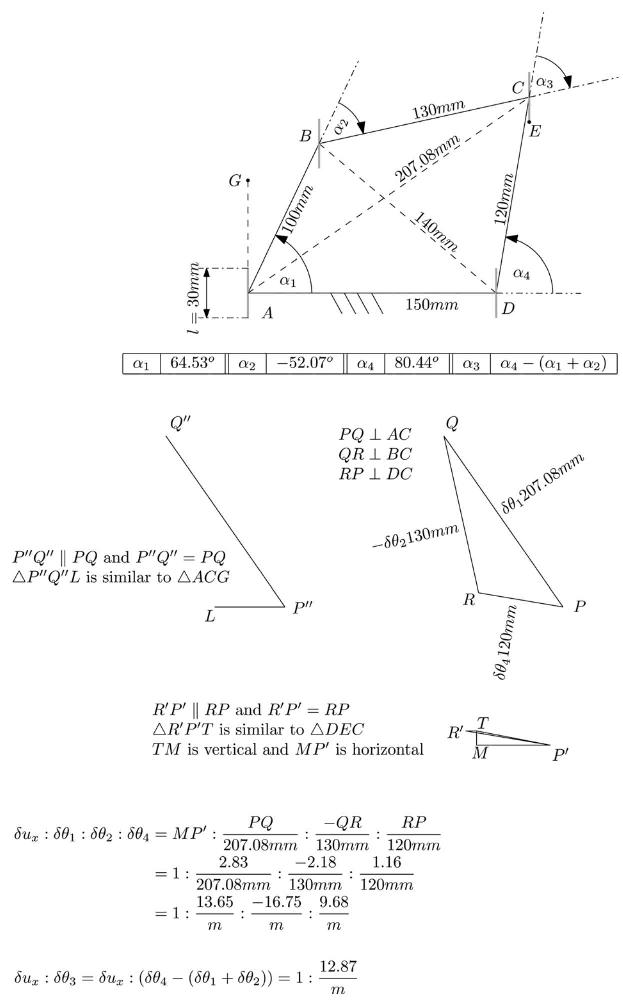

Fig. 9 Position and velocity analysis of the four-bar linkage in the reference (undeformed) configuration

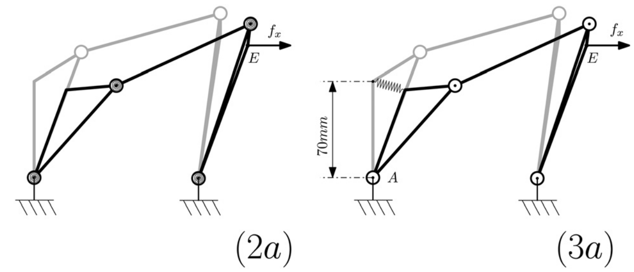

Fig. 10 Approximating torsional springs by zero-free-length springs

$$0 = \sum_{i=1}^{4} (-k_t \theta_i \delta\theta_i) + f_x \delta u_x \tag{18}$$

Hence, we have

$$f_x = \sum_{i=1}^{4} \left(k_t \theta_i \frac{d\theta_i}{du_x} \right) \tag{19}$$

Further, in the reference configuration ($\theta_i = 0$, for $i = 1 \cdots 4$), we have

$$\frac{df_x}{du_x} = k_t \sum_{i=1}^{4} \left(\frac{d\theta_i}{du_x} \right)^2 \tag{20}$$

Using $d\theta_i/du_x$ that is found from velocity analysis in Fig. 9 and the value of k_t evaluated in the table of Fig. 8, at the reference configuration, we get

$$\begin{aligned} \frac{df_x}{du_x} &= 2.85\,\mathrm{N/m} \left(13.65^2 + (-16.75)^2 + 12.87^2 + 9.68^2 \right) \frac{1}{\mathrm{m}^2} \\ &= 2070.1\,\mathrm{N/m} \end{aligned} \tag{21}$$

Calculation with more precision than what is given in Fig. 9 gives $df_x/du_x = 2061.1\,\mathrm{N/m}$. Thus, for case (2a), we have $f_x = 0\,\mathrm{N}$ and $df_x/du_x = 2061.1\,\mathrm{N/m}$ at the reference configuration.

In case (3a), let the deflection of the zero-free-length spring be represented by $\bar{\boldsymbol{u}}$. The virtual work equation, under the action of the external horizontal force f_x at point E and the zero-free-length spring, takes the following form:

$$0 = -k_z \bar{\boldsymbol{u}} \cdot \delta\bar{\boldsymbol{u}} + f_x \delta u_x \tag{22}$$

This implies that

$$f_x = k_z \bar{\boldsymbol{u}} \cdot \frac{d\bar{\boldsymbol{u}}}{du_x} \tag{23}$$

The derivative of f_x versus u_x at the reference configuration ($\bar{\boldsymbol{u}} = 0$) is given by

$$\frac{df_x}{du_x} = k_z \left(\frac{d\bar{\boldsymbol{u}}}{du_x} \right) \cdot \left(\frac{d\bar{\boldsymbol{u}}}{du_x} \right) \tag{24}$$

At the reference configuration, from the velocity triangles of Fig. 9, the horizontal component of $d\bar{\boldsymbol{u}}/du_x$ is LP''/MP' and the vertical component is zero. Hence $d\bar{\boldsymbol{u}}/du_x$ is $k_z(LP''/MP')^2$, which when measured from the velocity triangle becomes $0.912753k_z$.

At the reference configuration, the value of function f_x versus u_x is zero in both cases (2a) and (3a). In order to also have the derivative of the function, which is also a coefficient of first-order term in the Taylor's expansion, to be the same we get the equation $0.912753k_z = 2061.1$. From this equation, k_z the spring constant of the zero-free-length spring is solved as 2258.11 N/m. With this, all the parameters of the zero-free-length spring in case (3a) are evaluated.

2.3.4 Step 4—Perfect Static Balancing. In case (3a) (Fig. 10), the zero-free-length spring is anchored from the ground to a link that can kinematically be considered as a lever even though it is part of a four-bar linkage. Hence, the static balancing solution used for the lever of case (3a) (in Fig. 6) to obtain the lever of case (3b) can be applied here as well. The solution consists of adding a balancing zero-free-length spring which differs from the original spring in that the ground anchor point is radially opposite about the pivot of the lever. Application of this balancing solution is shown in Fig. 11(3*b*).

2.3.5 Step 5. The balancing spring of case (3b) is incorporated into case (1a) to obtain case (1b), as shown in Fig. 11. The expected approximate static balance in case (1b) may be judged from the plot of the effort function given in Fig. 12. A decrease in the effort to about 30% for case (1b) in comparison to case (1a) may be observed. In the plot, u_x spans over 0.05 m around *zero*. The plot was obtained through large-displacement linear elastic finite-element analysis. One may want to compare the magnitude of this span with the dimension of the smallest square box that bounds the entire mechanism and the balancing spring. The side of such a square box is about 0.2 m. Thus, the reduction of effort is obtained for a range of motion that is one-fourth of the size of the mechanism, which is substantial.

2.3.6 Prototype. A prototype was made to demonstrate the reduction in effort of the flexure-based compliant four-bar mechanism. A backside image of the prototype is shown in Fig. 13. The prototype deviates from the example in one important respect.

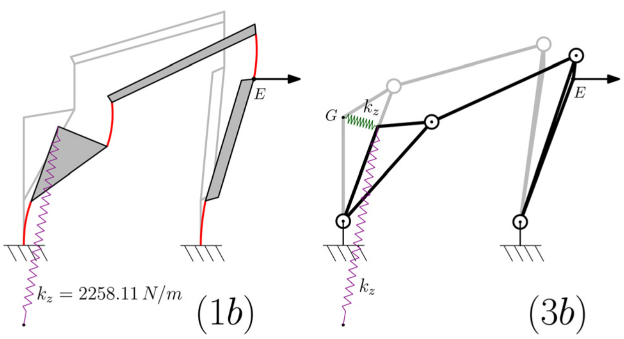

Fig. 11 Cases (3b) and (1b) in the analytical framework applied on the compliant four-bar linkage

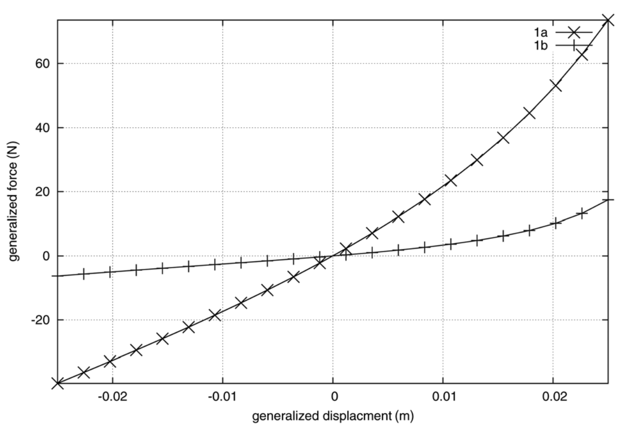

Fig. 12 Decrease in the effort function from case (1a) to case (1b)

Fig. 13 A prototype to demonstrate reduction in effort

It uses normal springs having finite free-length as balancing springs. In fact, four-balancing springs are used, which are mostly in parallel, except for little offset between anchor points. It may be verified that when zero-free-length spring is replaced by a nonzero-free-length spring in case (3b), the first-order balance is retained only when the spring force at the reference configuration for the latter spring matches that of the earlier spring. Therefore, the balancing springs were chosen such that the net force of all of them at the reference configuration is approximately the same as what is exerted by the balancing spring of case (1b) of Fig. 11. A provision has been made to change the number of active coils in the four springs. Since the number of active coils in the springs influences the force exerted by the springs, the number of active coils was used as a tuning parameter to tune the behavior of the prototype. During tuning, the following issues were noted:

(1) There is a significant shift in the equilibrium position of the prototype when the balancing springs are added.
(2) As the spring forces are increased by decreasing the number of active coils, the force deflection behavior loses its monotonicity and snap-through behavior sets in.

By tuning the number of active coils in the springs, the second issue was marginally eliminated and the equilibrium configuration was brought to the same configuration as that without balancing springs. After tuning, the four springs have spring constants of $\{0.68526, 0.62457, 0.50227, 0.50632\}$ N/mm with free-lengths of $\{72, 110, 77.5, 109\}$ mm, respectively. A single spring that is effectively equivalent to the four springs will have a spring constant of 2.32 N/mm and a free-length of 92 mm. An image of the prototype is shown in Fig. 13.

The force–deflection relation of the prototype, before and after the addition of the springs, is shown in Fig. 14. For the measurements, a force was applied by a spring balance attached to a thread that passes over the point E (see Fig. 11). The thread was maintained to be horizontal to ensure that the applied force is indeed horizontal.

From Fig. 14, it may be seen that the force required to deflect the prototype has reduced to about 40%. While making the prototype, we realized that practical considerations, such as availability of prestressed zero-free-length springs, prevented the prototype from accurately capturing the theoretical case. Furthermore, it was shown in Ref. [19] that high loads on the flexure due to balancing springs can change the torsional stiffness of flexure. Our framework does not take into account the effect of high loads on the flexure due to balancing springs. In spite of these, we expected the prototype to demonstrate a significant reduction in force even though the reduction may not be as good as the analytical prediction. To that extent, the prototype has demonstrated reduction in actuation effort.

2.4 A Compliant "Two Degree-of-Freedom" Probe.

Figure 15 shows a flexure-based compliant probe at P. While in Fig. 6 point P had very high stiffness in the vertical direction compared to horizontal direction, here the stiffness of point P is comparable in all the directions of the plane. Hence, we are calling it a two degree-of-freedom probe. We now apply the analytical framework on this example.

2.4.1 Step 1. The function $\boldsymbol{f}$ versus $\boldsymbol{u}$ is taken as the effort function, where $\boldsymbol{u}$ is the displacement of point P for an applied force of $\boldsymbol{f}$ on point P, as could be seen in Fig. 15(1a). It may be noted that unlike previous examples where the function was from the set of real numbers to the set of real numbers, here it is a function from the set of two-dimensional real vectors to the set of two-dimensional real vectors.

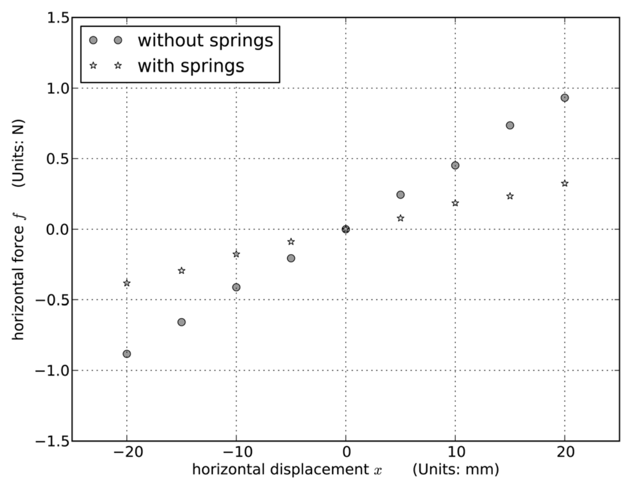

Fig. 14 Force deflection relationship of the prototype

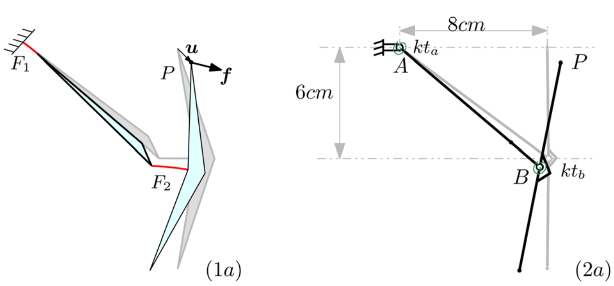

Fig. 15 A two degree-of-freedom compliant pointer and its approximation as a rigid-body linkage loaded by torsional springs

2.4.2 Step 2. The small-length flexure approximation is applied on the compliant probe to obtain a 2R linkage loaded by torsional springs, as shown in Fig. 15(2a). In the reference configuration, which corresponds to the undeformed configuration of the compliant probe, the centers of the pivot A, B, and point P form a right angled triangle corresponding to the Pythagorean triplet $\{3, 4, 5\}$, as shown in Fig. 15(2a). Calculation of the torsional-spring constants from the flexure details is given in Table 1.

2.4.3 Step 3. It is proposed to approximate the torsional springs by zero-free-length springs, as shown in Fig. 16. There are two zero-free-length springs: one attached to link AB and the other attached to link BP. In the reference configuration, both the zero-free-length springs are undeformed, i.e., their anchor points coincide. While for the first spring, the anchor points are at the coordinates of $(6.4\,\mathrm{cm}, -4.8\,\mathrm{cm})$, and the anchor points of the second spring are at point P. The point at which the first spring anchors to the linkage is labeled as E. In order to obtain the spring constants of these springs (k_1 and k_2), we find the effort function $\boldsymbol{f}$ versus $\boldsymbol{u}$ in cases (2a) and (3a).

Case (2a). The virtual work equilibrium equation in case (2a) takes the following form:

$$0 = -k_{ta}\theta_a\delta\theta_a - k_{tb}\theta_b\delta\theta_b + \boldsymbol{f}\cdot\boldsymbol{\delta u} \tag{25}$$

Equation (25) may be rewritten in the following form:

$$(\boldsymbol{K_t\theta})^{\mathrm{T}}\boldsymbol{\delta}\theta = \boldsymbol{f}^{\mathrm{T}}\boldsymbol{\delta u} \tag{26}$$

where

$$\boldsymbol{\theta} = \begin{bmatrix}\theta_a\\ \theta_b\end{bmatrix},\quad \boldsymbol{K_t} = \begin{bmatrix}k_{ta} & 0\\ 0 & k_{tb}\end{bmatrix},\quad \boldsymbol{f} = \begin{bmatrix}f_a\\ f_b\end{bmatrix},\quad \text{and}\quad \boldsymbol{u} = \begin{bmatrix}u_x\\ u_y\end{bmatrix}$$

Let $\boldsymbol{\nabla_u}\theta$ represent the derivative of $\boldsymbol{\theta}$ with respect to $\boldsymbol{u}$. Then, using the arbitrariness of $\boldsymbol{\delta u}$, Eq. (26) may be rewritten as

$$(\boldsymbol{K_t\theta})^{\mathrm{T}}\boldsymbol{\nabla_u}\theta = \boldsymbol{f}^{\mathrm{T}} \qquad \text{or} \qquad \boldsymbol{f} = (\boldsymbol{\nabla_u}\theta)^{\mathrm{T}}\boldsymbol{K_t\theta} \tag{27}$$

Table 1 Details of flexure and calculation of torsional-spring constant

E	Young's modulus	205×10^{9} (Pa)
h	Height of the flexure cross section	500×10^{-6} (m)
b	Width of flexure cross section	4×10^{-2} (m)
I	Area moment of inertia $= bh^3/12$	4.1667×10^{-13} (m^4)
l_a	Length of flexure corresponding to pivot A	1×10^{-2} (m)
l_b	Length of flexure corresponding to pivot B	2×10^{-2} (m)
k_{ta}	Torsional-spring constant $= EI/l_a$	8.541667 (N·m)
k_{tb}	Second torsional-spring constant $= EI/l_b$	4.270833 (N·m)

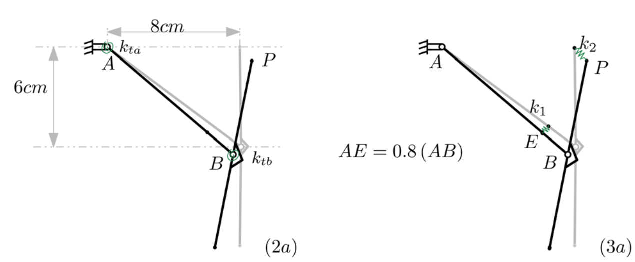

Fig. 16 Cases (2a) and (3a) in the analytical framework applied on two degree-of-freedom probe

Further, from Eq. (27), the derivative of $\boldsymbol{f}$ with respect to $\boldsymbol{u}$ at the reference configuration ($\boldsymbol{\theta} = 0$) becomes

$$\nabla_{\boldsymbol{u}} \boldsymbol{f} = (\nabla_{\boldsymbol{u}} \theta)^{\mathrm{T}} \boldsymbol{K}_t (\nabla_{\boldsymbol{u}} \theta) \tag{28}$$

From the velocity analysis of the linkage, it follows that

$$\begin{aligned}(\nabla_\theta \boldsymbol{u}) = (\nabla_{\boldsymbol{u}} \theta)^{-1} &= \begin{bmatrix} 0 & -(BP)_{\mathrm{ref}} \\ AP_{\mathrm{ref}} & 0 \end{bmatrix} \\ &= \begin{bmatrix} 0 & -6 \times 10^{-2}\,\mathrm{m} \\ 8 \times 10^{-2}\,\mathrm{m} & 0 \end{bmatrix}\end{aligned} \tag{29}$$

where BP_{ref} and AP_{ref} indicate the lengths of segments BP and AP in the reference configuration. Substituting for $\nabla_{\boldsymbol{u}} \theta$ from Eq. (29) and for k_{ta} and k_{tb} from Table 1 into Eq. (28), we get

$$\nabla_{\boldsymbol{u}} \boldsymbol{f} = \begin{bmatrix} 1186.342 & 0 \\ 0 & 1334.635 \end{bmatrix} (\mathrm{N/m}) \tag{30}$$

Case (*3a*). Let the displacement of point E, where the first zero-free-length spring is attached, be represented by $\bar{\boldsymbol{u}}$. The virtual work equilibrium equation in case (3a) takes the following form:

$$0 = -k_1 \boldsymbol{\delta} \bar{\boldsymbol{u}}^{\mathrm{T}} \bar{\boldsymbol{u}} - k_2 \boldsymbol{\delta} \boldsymbol{u}^{\mathrm{T}} \boldsymbol{u} + \boldsymbol{\delta} \boldsymbol{u}^{\mathrm{T}} \boldsymbol{f} \tag{31}$$

Let $\nabla_{\boldsymbol{u}} \bar{\boldsymbol{u}}$ represent the derivative of $\bar{\boldsymbol{u}}$ with respect to $\boldsymbol{u}$. Then, Eq. (31) may be solved for $\boldsymbol{f}$ as

$$\boldsymbol{f} = k_1 (\nabla_{\boldsymbol{u}} \bar{\boldsymbol{u}})^{\mathrm{T}} \bar{\boldsymbol{u}} + k_2 \boldsymbol{u} \tag{32}$$

The derivative of $\boldsymbol{f}$ with respect to $\boldsymbol{u}$ at the reference configuration ($\boldsymbol{u} = 0$ and $\bar{\boldsymbol{u}} = 0$) becomes

$$\nabla_{\boldsymbol{u}} \boldsymbol{f} = k_1 (\nabla_{\boldsymbol{u}} \bar{\boldsymbol{u}})^{\mathrm{T}} (\nabla_{\boldsymbol{u}} \bar{\boldsymbol{u}}) + k_2 \boldsymbol{I} \tag{33}$$

where $\boldsymbol{I}$ is the 2×2 identity matrix. From the velocity analysis at the reference configuration, it follows that

$$\nabla_\theta \bar{\boldsymbol{u}} = \begin{bmatrix} 0.8 \times 6 & 0 \\ 0.8 \times 8 & 0 \end{bmatrix} \times 10^{-2}\mathrm{m}, \quad \nabla_\theta \boldsymbol{u} = \begin{bmatrix} 0 & -6 \\ 8 & 0 \end{bmatrix} \times 10^{-2}\mathrm{m} \tag{34}$$

From calculus, it follows that

$$\nabla_{\boldsymbol{u}} \bar{\boldsymbol{u}} = \nabla_\theta \bar{\boldsymbol{u}} (\nabla_\theta \boldsymbol{u})^{-1} = \frac{0.8}{8} \begin{bmatrix} 0 & 6 \\ 0 & 8 \end{bmatrix} \tag{35}$$

Substituting Eq. (35) in Eq. (33), we get

$$\nabla_{\boldsymbol{u}} \boldsymbol{f} = \begin{bmatrix} k_2 & 0 \\ 0 & k_1 + k_2 \end{bmatrix} \tag{36}$$

Finding k_1 and k_2. At the reference configuration, $\boldsymbol{f} = 0$ in both cases (2a) and (3a). In order to also have the first-order terms of the Taylor's expansion of $\boldsymbol{f}$ versus $\boldsymbol{u}$ to be the same, we equate $\nabla_{\boldsymbol{u}} \boldsymbol{f}$ from case (2a) (Eq. (30)) and case (3a) (Eq. (36)) to solve for k_1 and k_2 as

$$k_2 = 1186.342\,\mathrm{N/m}, \quad \text{and} \quad k_1 = 148.293\,\mathrm{N/m} \tag{37}$$

2.4.4 Step 4. The linkage and the two springs in Fig. 16(3*a*) are exactly same as the linkage and the springs $\mathcal{Z}_1^{[1]}$ and $\mathcal{Z}_1^{[2]}$ of Fig. 2. As demonstrated in Fig. 2, incorporation of two more springs $\mathcal{Z}_2^{[1]}$ and $\mathcal{Z}_2^{[2]}$, the details of which are given in the same figure, will lead to perfectly statically balanced linkage. These springs are added to case (3a) to obtain case (3b), as shown in Fig. 17.

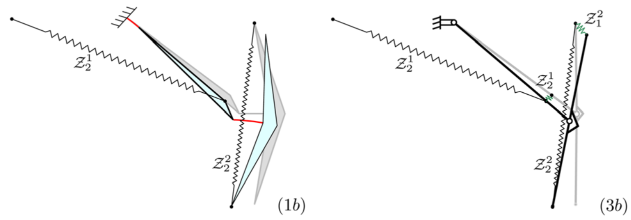

Fig. 17 Cases (3b) and (1b) of the analytical framework applied on the two degree-of-freedom compliant probe

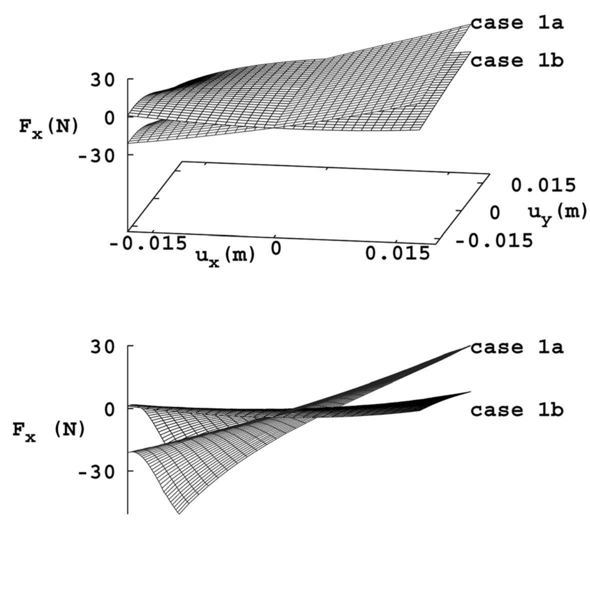

Fig. 18 f_x versus u plot in two different views

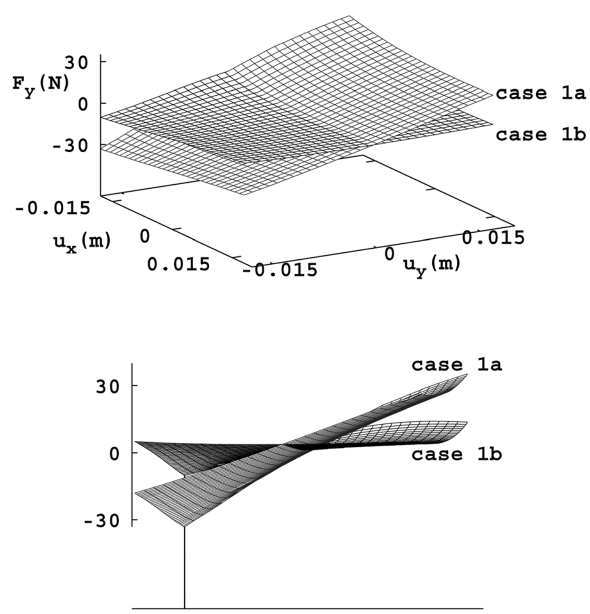

Fig. 19 f_y versus u plot in two different views

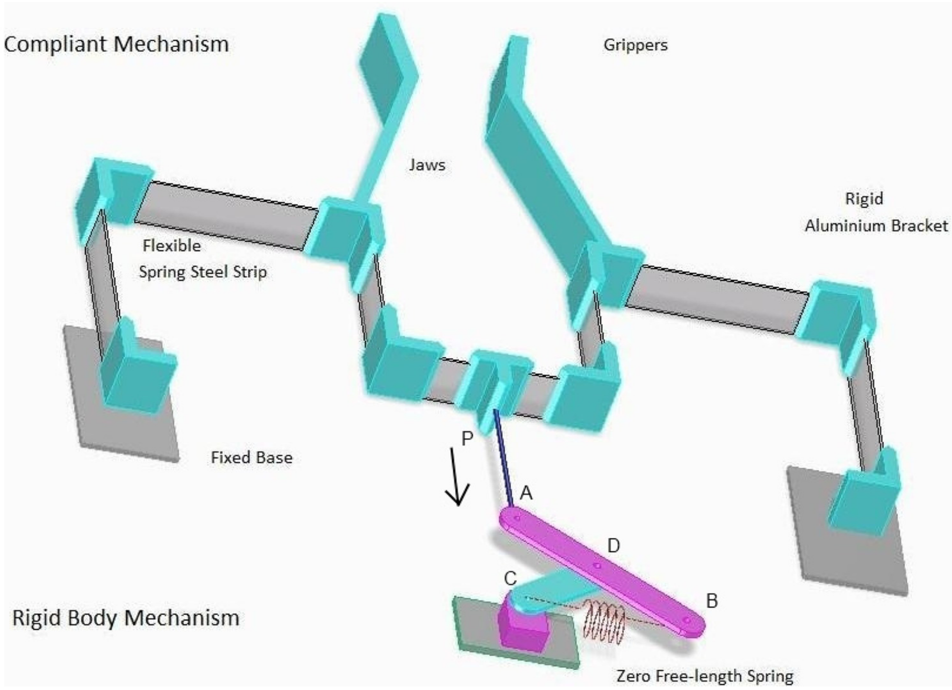

Fig. 20 Graphical representation of the gripper

2.4.5 Step 5. The balancing springs $\mathcal{Z}_2^{[1]}$ and $\mathcal{Z}_2^{[2]}$ of case (3b) are incorporated into case (1a) to obtain case (1b), as shown in Fig. 17(1*b*). The expected decrease in the effort function may be judged from Figs. 18 and 19, which show f_x versus $\boldsymbol{u}$ and f_y versus $\boldsymbol{u}$ for both cases (1a) and (1b). It may be noted that in most regions, the effort function for case (1b) is less than 30% of that of case (1a). The largest deflection considered for $\boldsymbol{u}$ is about 20% of the overall size of the arrangement of case (1b). These plots were obtained from finite-element simulation using linear elastic model with geometric nonlinearity.

2.5 Discussion. As could be noted from the results of Sec. 2, the analytical framework leads to only approximate static balance. However, one can run a numerical optimization on the parameters of the balancing springs to further reduce the effort function. One can also replace zero-free-length springs by normal springs or compliant elements that would approximately exert similar forces. This could be followed by an optimization on the parameters of the normal springs or compliant elements with the objective of reducing the effort function. In this paper, apart from the prototype where normal springs were used, we do not demonstrate such an optimization since the intent of the framework is to provide tools that help a designer to conceptualize new statically balanced configurations. It is for this reason that the framework is kept simple and analytical with almost all its steps being amenable to imagination of a mechanical designer.

3 Static Balancing of Compliant Mechanisms Using Rigid-Body Linkages and Springs

While the earlier examples showed the applicability of the method presented in the paper, we now consider another way of utilizing static balance of rigid-body linkages for balancing a compliant mechanism. Here, a compliant mechanism is modeled as a load spring of a rigid-body linkage.

Figure 20 shows a geometric model of the gripper. The gray portions are made of spring steel and the connecting brackets, which have higher thickness, are made of aluminum. Deformation takes places only in the spring-steel regions because their cross section areas are much smaller compared to that of the aluminum brackets. Figure 21 shows the schematic of only the static-balancing linkage with its balancing spring k_2. In this, the compliant mechanism is modeled as a linear translational spring, k_1. This modeling is valid for a small range of motion. Therefore, the compliant mechanism is made to be large in size as compared to the balancing linkage. It should be noted that the entire compliant mechanism is simply a “loading spring” for the rigid-body linkage.

The linkage in Fig. 21 is statically balanced if [14]

$$k_1 l_1 = k_2 l_2 \tag{38}$$

Thus, by using a two body linkage and a balancing spring k_2 in accordance with Eq. (38), we can balance a relatively large compliant mechanism.

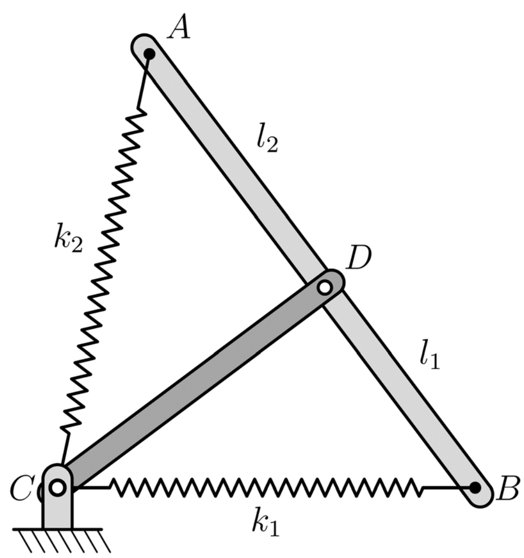

Fig. 21 Planar representation of the model

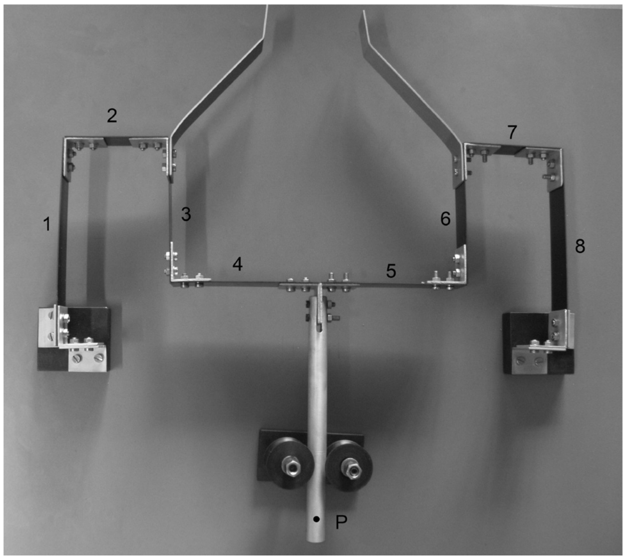

Fig. 22 Compliant metallic gripper without static balancing

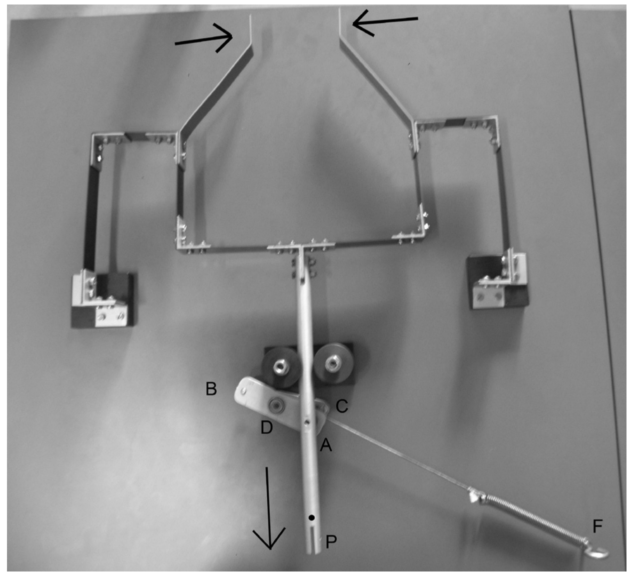

Fig. 24 Compliant metallic gripper with static balancing

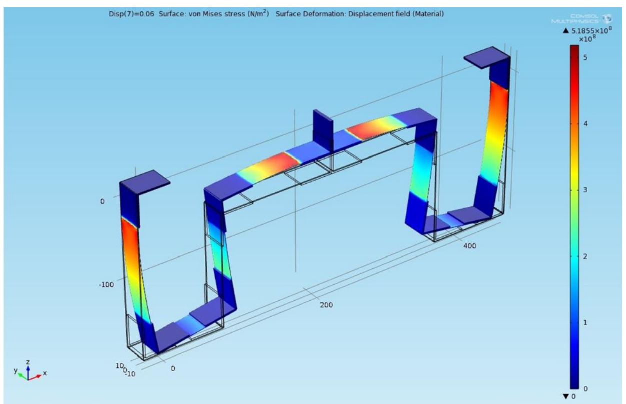

Fig. 23 Finite-element analysis of the model using COMSOL

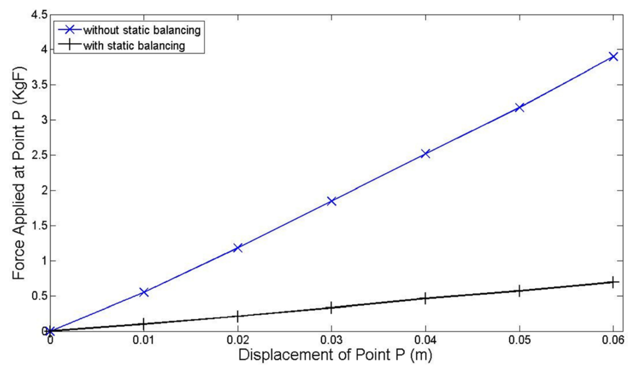

Fig. 25 Comparison of force–displacement relation of point *P* without and with static balancing

3.1 Design. Spring-steel strips of 1 mm thickness and lengths of 180 mm (strips 1 and 8), 140 mm (strips 3–6), and 100 mm (strips 2 and 7) were cut and assembled as in Fig. 22. The corner bracket elements as shown in the figure are of aluminum and have a uniform thickness of 3 mm and arm length of 40 mm on each side.

The length of rigid link *AB* was assumed to be 80 mm with the center at D. According to Eq. (38), the length of link *CD* was fixed at 40 mm. The stiffness constant of spring *CB* was fixed at 550 N/m. The deductions and explanation for these assumptions are given in Sec. 3.2. The following data are used in the further calculations:

- Young's modulus of spring steel = 200 GPa
- Young's modulus of aluminum = 70 GPa
- Yield stress of spring steel = 550 MPa
- Yield stress of aluminum = 120 MPa
- Factor of safety for aluminum and spring-steel parts = 1

3.2 Linear Behavior and Displacement Range. Since our main concern was to reduce the effort to deform the mechanism, we concentrated only on forces and displacements of point *P* (Fig. 20). Before calculating the forces, it was important to first obtain the displacement range of the gripper within which the mechanism displayed linear behavior, i.e., the force–displacement curve is linear. Therefore, the model was simulated using a finite-element software[1] and the maximum displacement of point *P* within linearity was found to be 60 mm (Fig. 23).

Further, the reaction forces at point *P* were calculated as well to obtain the spring characteristics of the compliant mechanism. This was used to select and tune the finite-length spring while simultaneously satisfying the governing principle in Eq. (38).

To avoid the rigid-body linkage from reaching a singular configuration, the maximum deflection of zero-free-length spring *BC* was required to have a value greater than the length of link *CD*. Conversely, the length of link *CD* had to be assumed such that it was less than the maximum spring deflection. Since the deflection of the spring depends on linear characteristics of the compliant mechanism, it can be seen that the length of link *CD* has to be less than the deduced value of 60 mm. Therefore, as mentioned in Sec. 3.1 and according to Eq. (38), the lengths of *AB* and *CD* were assumed to be 80 mm and 40 mm, respectively.

3.3 Fabrication. While assembling the rigid-body linkages and the spring according to the planar representation given in Fig. 21, care was taken to incorporate the equivalence between the finite-length spring and the theoretical zero-free-length spring. For this, an arrangement shown in Fig. 24 was made, where the fixed anchor point of the spring was considered to be a different point *F* in the workspace. Further, it was ensured that the

[1] www.comsol.com

inextensible string (a nylon thread) connecting points B and F passed over point C at all times by making the string pass between two small, parallel frictionless rollers assembled on link CD and exactly over point C. Further, the actuator link containing point P was made to pass through two big frictionless parallel rollers to ensure that the applied force and displacement of point P were unidirectional (perpendicular to gripper action), as shown in Fig. 24. All rolling and rotating actions were realized through high-quality roller bearings.

It is can be observed from Fig. 25 that the effort needed to deflect the compliant mechanism within its linear action domain is reduced by three-fourths. However, according to the theory, the effort should have been zero with static balancing. This deviation from the theoretical case may be attributed to: (a) error in realizing a zero-free-length spring from a finite-length spring and (b) error in the perpendicular alignment of direction of applied force with the gripper action direction. Further, in spite of using low-friction bearings, frictional effects such as hysteresis may be present.

4 Conclusion

In this paper, we presented a simple analytical framework to conceptualize solutions for static balancing of flexure-based compliant systems. The framework employed two approximations: small-length flexure-based pseudo-rigid-body model and approximation of torsional springs by zero-free-length springs. These approximations were used in conjunction with known analytical perfect balancing techniques for rigid-body linkages loaded by zero-free-length springs. The static balancing solution involves addition of zero-free-length springs to the compliant systems. The framework was illustrated on three flexure-based compliant systems. The effectiveness of the framework was judged through finite-element simulations as well as a prototype. The analytical framework was kept simple so that it is amenable to the imagination of a designer, which in turn helps the designer to be creative. The solution obtained from the framework could be made more practical by replacing balancing zero-free-length springs by more realistic force exerting elements followed by a numerical optimization.

Additionally, a balancing example was also demonstrated where balancing was accomplished by addition of both rigid-body linkages and springs. Such a balancing could be useful when the usage of rigid-body linkages does not deteriorate the overall performance of a compliant system. Thus, based on the two approaches presented here, we showed that compliant mechanisms can be approximately balanced by deriving insights from analytical perfect static balancing techniques developed for rigid-body linkages.

References

[1] Howell, L. L., 2001, *Compliant Mechanisms*, Wiley, New York.
[2] Herder, J. L., and van den Berg, F. P. A., 2000, "Statically Balanced Compliant Mechanisms (SBCMs), an Example and Prospects," ASME Paper No. DETC2000/MECH-14144.
[3] Stapel, A., and Herder, J. L., 2004, "Feasibility Study of a Fully Compliant Statically Balanced Laparoscopic Grasper," ASME Paper No. DETC2004-57242.
[4] de Lange, D. J. B. A., Langelaar, M., and Herder, J. L., 2008, "Towards the Design of a Statically Balanced Compliant Laparoscopic Grasper Using Topology Optimization," ASME Paper No. DETC2008-49794.
[5] Tolou, N., and Herder, J. L., 2009, "Concept and Modeling of a Statically Balanced Compliant Laparoscopic Grasper," ASME Paper No. DETC2009-86694.
[6] Rosenberg, E. J., Radaelli, G., and Herder, J. L., 2010, "An Energy Approach to a 2DOF Compliant Parallel Mechanism With Self-Guiding Statically-Balanced Straight-Line Behavior," ASME Paper No. DETC2010-28447.
[7] Hoetmer, K., Woo, G., Kim, C., and Herder, J., 2010, "Negative Stiffness Building Blocks for Statically Balanced Compliant Mechanisms: Design and Testing," ASME J. Mech. Rob., **2**(4), p. 041007.
[8] Morsch, F. M., and Herder, J. L., 2010, "Design of a Generic Zero Stiffness Compliant Joint," ASME Paper No. DETC2010-28351.
[9] Gallego, J. A., and Herder, J. L., 2010, "Criteria for the Static Balancing of Compliant Mechanisms," ASME Paper No. DETC2010-28469.
[10] Tolou, N., and Herder, J. L., 2010, "Statically Balanced Compliant Micro Mechanisms (SM-MEMS): Concepts and Simulation," ASME Paper No. DETC2010-28406.
[11] Dunning, A. G., Tolou, N., and Herder, J. L., 2011, "Review Article: Inventory of Platforms Towards the Design of a Statically Balanced Six Degrees of Freedom Compliant Precision Stage," Mech. Sci., **2**(2), pp. 157–168.
[12] Chen, G., and Zhang, S., 2011, "Fully-Compliant Statically-Balanced Mechanisms Without Prestressing Assembly: Concepts and Case Studies," Mech. Sci., **2**(2), pp. 169–174.
[13] Herder, J. L., 1998, "Design of Spring Force Compensation Systems," Mech. Mach. Theory, **33**(1), pp. 151–161.
[14] Herder, J. L., 2001, "Energy-Free Systems: Theory, Conception and Design of Statically Balanced Spring Mechanisms," Ph.D. dissertation, Delft University of Technology, Delft, The Netherlands.
[15] Deepak, S. R., and Ananthasuresh, G., 2012, "Static Balancing of a Four-Bar Linkage and Its Cognates," Mech. Mach. Theory, **48**, pp. 62–80.
[16] Deepak, S., and Ananthasuresh, G. K., 2009, "Static Balancing of Spring-Loaded Planar Revolute-Joint Linkages Without Auxiliary Links," 14th National Conference on Machines and Mechanisms (NaCoMM09), NIT, Durgapur, India, Dec. 17–18, Paper No. NaCoMM-2009-ASMSD20, pp. 37–44.
[17] Deepak, S. R., and Ananthasuresh, G. K., 2012, "Perfect Static Balance of Linkages by Addition of Springs but not Auxiliary Bodies," ASME J. Mech. Rob., **4**(2), p. 021014.
[18] Radaelli, G., Gallego, J. A., and Herder, J. L., 2011, "An Energy Approach to Static Balancing of Systems With Torsion Stiffness," ASME J. Mech. Des., **133**(9), p. 091006.
[19] Merriam, E. G., and Howell, L. L., 2015, "Non-Dimensional Approach for Static Balancing of Rotational Flexures," Mech. Mach. Theory, **84**, pp. 90–98.
[20] Howell, L. L., and Midha, A., 1994, "A Method for the Design of Compliant Mechanisms With Small-Length Flexural Pivots," ASME J. Mech. Des., **116**(1), pp. 280–290.
[21] Mabie, H., and Reinholtz, C., 1987, *Mechanisms and Dynamics of Machinery*, Wiley, New York.